# INFLUENCE OF HEAT IN-LEAK, LONGITUDINAL CONDUCTION AND PROPERTY VARIATIONS ON THE PERFORMANCE OF CRYOGENIC PLATE-FIN HEAT EXCHANGERS BASED ON DISTRIBUTED PARAMETER MODEL

***Qingfeng Jiang*** [a,b,*], ***Ming Zhuang*** [a], ***Zhigang Zhu*** [a], ***Linhai Sheng*** [a], ***Ping Zhu*** [a]

[a] Institute of Plasma Physics, Chinese Academy of Sciences, Hefei, Anhui 230031, China

[b] University of Science and Technology of China, Hefei, Anhui 230026, China

[*] Corresponding author; E-mail: qfjiang@ipp.ac.cn

*For helium liquefaction/refrigeration systems, conventional design theory always fails in cryogenic applications and heat exchangers operating at low temperatures are usually sensitive to longitudinal heat conduction, heat in-leak from surroundings and variable fluid properties. Governing equations based on distributed parameter methods are developed to evaluate performance deterioration caused by these effects. The model synthetically considering these loss mechanisms is validated against experimental data and design results obtained by commercial software Aspen MUSE*$^{TM}$*. Sample multi-stream heat exchangers are further studied to discuss quantitative effects of these heat losses. In accordance with previous researches, the comprehensive effects of various losses are analyzed qualitatively in order to reveal their influences and investigate on the strategies of improving the heat transfer performance. The numerical method is useful in the design procedure of cryogenic heat exchangers and can be adopted to predict heat transfer and pressure drop performance under the actual low-temperature environment.*

Key words: *heat exchanger, longitudinal conduction, heat in-leak, helium liquefier, helium refrigerator*

## Introduction

Counter-flow plate-fin heat exchangers (PFHEs) are commonly utilized in cryogenic applications due to their high effectiveness and compact size. In helium liquefaction/refrigeration systems, PFHEs are always used to further cool the coming hot and high-pressure helium gas by recuperating most sensible heat from the low-pressure vapor. However, for the cryogenic applications, various parameters such as longitudinal heat conduction, heat-in-leak from surroundings and property variations of fluid need to be considered carefully, which are often neglected in the conventional design procedure of heat exchangers. Lumped parameter models, as the basic design theory, i.e. the effectiveness–number of heat transfer units ($\varepsilon - NTU$) method, the logarithmic mean temperature difference (*LMTD*) method and so on, are based on the assumptions of steady-state, negligible heat transfer from ambient, no longitudinal heat conduction, constant heat capacity rate, constant individual and overall heat transfer coefficients [1,2]. When the magnitude of these secondary parameters is too

large to be neglected, these closed form solutions wouldn't be precise enough.

During the last several decades, these effects have been studied by many researchers based on various different assumptions. For the performance deterioration caused by longitudinal heat conduction, which would flatten the temperature distributions in the wall and thus reduce the effectiveness, Kays and London [1] provided graphical results for the balanced and imbalanced counter-flow heat exchangers. More comprehensive, systematic analytical results assuming constant properties and adiabatic end conditions were proposed by Kroeger [3]. For the conditions of the heat exchanger cold end directly connected to the evaporator in Joule–Thomson refrigerators, Narayanan and Venkatarathnam [4] discussed the parasitic heat loss through the wall at the cold end. Hansen [5] investigated the effects of longitudinal conduction and found that there exists an optimal metal conductivity for the geometry considered in the design of heat exchangers incorporated with J–T expansion process. Krishna [6] studied the effect of longitudinal wall conduction on the performance of three-fluid cryogenic heat exchangers. Saberimoghaddam [7] found that the higher tube wall thermal conductivity would not bring about a bigger temperature measurement error at tube outlet, while the wall thermal conductivity leaded to longitudinal conduction in the tube wall.

In addition, a significant amount of heat in-leak from ambient could be crucial in determining the heat exchanger performance. Chowdhury and Sarangi [8] analyzed a heat exchanger exposed to a parasitic heat transfer that is driven by a temperature difference between a fixed ambient temperature and the local fluid temperature. Gupta and Atrey [9] published the experimental results and numerical modeling considering the heat in-leak from surroundings and longitudinal conduction through the wall. Based on this model, the characterizations of various losses were discussed by Aminuddin and Zubair [10] assuming adiabatic and nonadiabatic end conditions. Different from the assumptions of external heat transfer linearly proportional to the temperature difference between ambient and fluid, Nellis [11] considered radiative heat transfer as the dominant parasitic in a typical cryogenic heat exchanger. The commercial software, Aspen MUSE$^{TM}$ [12], has been successfully used to evaluate the performance of PFHEs. It can effectively take into accounts the losses due to longitudinal conduction and actual fluid physical properties, but the heat in-leak is empirically represented as a rough input from any source.

In order to study these combined effects, many numerical models have been developed. A systematic review of the evolution and challenges in mathematical models of cryogenic heat exchangers was presented by Pacio and Dorao [13]. The differential equations derived by Kroeger [3] under conditions of constant properties could be used to study the effects of longitudinal conduction for balanced and imbalanced flow qualitatively and systematically. Gupta and Atrey [9,14] extended the model to cover heat in-leak from surroundings. The numerical model presented by Nellis [11] considering the effects of property variations, metal conductivity, parasitic heat load, and heat transfer coefficients was useful in the design of a two-stream heat exchangers. To take care of transverse heat conduction for multi-stream heat exchangers, Goyal [15] presented a detailed numerical model with discretizing energy balance equations additionally for fin elements.

In this study, the model early proposed is modified at the methodology of analysis and modeling, which can not only reveal the cryogenic loss mechanisms qualitatively, but also analyze the quantitative effects of these losses occurring in multi-stream heat exchangers under the actual cryogenic environment. Based on the model, the predictions are validated against experimental results presented previously. To further examine the flexibility of this model and overcome the insufficiencies of the commercial software, the results about two integrated common cases with special reference to

helium liquefaction/refrigeration systems are made comparisons with the predictions. The numerical model could be useful for designers to properly forecast the performance deterioration under conditions of considering arbitrary variations of number of transfer units, heat capacity ratios, fluid properties, metal conductivities, parasitic heat loads, heat transfer and frictional resistance coefficients along the length of heat exchangers. Compared with studies reported in previous literatures, qualitative analyses of performance influences caused by longitudinal heat conduction, heat in-leak and property variations are also performed for different number of transfer units and heat capacity rate ratios.

## 2. Numerical model

In this section, governing equations for a counter-flow heat exchanger with external heat transfer to the cold fluid are derived based on the conservation of energy in a control volume and expressed in dimensionless form by commonly used parameters. The computational grid consisting of the necessary nodes and elements is illustrated in Fig.1. Considering the effects of longitudinal conduction tend to be concentrated at the ends, an exponentially distributed grid [11], $\gamma = 4$, characterized by higher concentration of nodes near the edges is applied. The heat exchanger is divided into *n* sections. Each section consists of three elements: hot fluid side, cold fluid side and wall boundary. With the following assumptions:

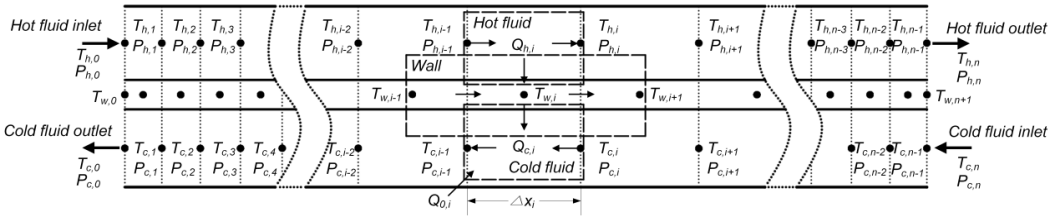


**Fig. 1.** Computational grid for the numerical model

i. Steady-state conditions exist throughout the heat exchanger.
ii. In any cross-section for every passage, the fluid temperature and pressure perpendicular to the flow direction remain unchanged.
iii. The metal matrix temperature inside the core is constant along the width of the heat exchanger.
iv. The fluid in every passage is distributed uniformly.
The governing equations in the *i*th section are as follows:
*Hot fluid:*

$$\frac{U_{h,i}+U_{h,i-1}}{2}A'_{s,h}\Delta x_i\left(\frac{T_{h,i}+T_{h,i-1}}{2}-T_{w,i}\right)+U_{0,hi}A_{0,hi}(T_a-\frac{T_{h,i}+T_{h,i-1}}{2})=\frac{C_{h.i}+C_{h,i-1}}{2}(T_{h,i-1}-T_{h,i}) \quad (1)$$

*Wall:*

$$\frac{U_{h,i}+U_{h,i-1}}{2}A'_{s,h}\Delta x_i\left(\frac{T_{h,i}+T_{h,i-1}}{2}-T_{w,i}\right)+\frac{(k_{w,i-1}+k_{w,i})\,A_c}{\Delta x_i+\Delta x_{i-1}}\left(T_{w,i-1}-T_{w,i}\right)+U_{0,wi}A_{0,wi}(T_a-$$

$$\frac{T_{w,i-1}+T_{w,i+1}}{2})=\frac{U_{c,i}+U_{c,i-1}}{2}A'_{s,c}\Delta x_i\left(T_{w,i}-\frac{T_{c,i}+T_{c,i-1}}{2}\right)+\frac{(k_{w,i}+k_{w,i+1})\,A_c}{\Delta x_i+\Delta x_{i+1}}(T_{w,i}-T_{w,i+1}) \quad (2)$$

*Cold fluid:*

$$\frac{U_{c,i}+U_{c,i-1}}{2}A'_{s,c}\Delta x_i\left(T_{w,i}-\frac{T_{c,i}+T_{c,i-1}}{2}\right)+U_{0,ci}A_{0,ci}(T_a-\frac{T_{c,i}+T_{c,i-1}}{2})=\frac{C_{c.i}+C_{c,i-1}}{2}(T_{c,i-1}-T_{c,i}) \quad (3)$$

The above energy equations can be analyzed non-dimensionally:

*Hot fluid:*

$$(\frac{v_{h,i}\,\Delta \mathrm{X}_i}{v_{h,i-1}\,\Delta \mathrm{X}_{i-1}} ntu_{h,i-1} + ntu_{h,i}) \left(\frac{\theta_{h,i}+\theta_{h,i-1}}{2} - \theta_{w,i}\right) + 2\alpha_{hi} NTU_i v_{h,i} (R - \frac{\theta_{h,i}+\theta_{h,i-1}}{2} + 1) =$$

$$\frac{\mu_{h.i}+\mu_{h,i-1}}{\mu_{h.i}} (\theta_{h,i-1} - \theta_{h,i}) \tag{4}$$

*Wall:*

$$(\frac{\Delta \mathrm{X}_i}{v_{h,i-1}\Delta \mathrm{X}_{i-1}} ntu_{h,i-1} + \frac{1}{v_{h,i}} ntu_{h,i}) \left(\frac{\theta_{h,i}+\theta_{h,i-1}}{2} - \theta_{w,i}\right) + 2\frac{\lambda_{i-1}+\lambda_i}{\Delta X_{i-1}+\Delta X_i} (\theta_{w,i-1} - \theta_{w,i}) + 2\alpha_{wi} NTU_i (R -$$

$$\frac{\theta_{w,i-1}+\theta_{w,i+1}}{2} + 1) = (\frac{\Delta \mathrm{X}_i}{v_{c,i-1}\,\Delta \mathrm{X}_{i-1}} ntu_{c,i-1} + \frac{1}{v_{c,i}} ntu_{c,i}) \left(\theta_{w,i} - \frac{\theta_{c,i}+\theta_{c,i-1}}{2}\right) + 2\frac{\lambda_i+\lambda_{i+1}}{\Delta X_i+\Delta X_{i+1}} (\theta_{w,i} - \theta_{w,i+1}) \tag{5}$$

*Cold fluid:*

$$(\frac{v_{c,i}\,\Delta \mathrm{X}_i}{v_{c,i-1}\,\Delta \mathrm{X}_{i-1}} ntu_{c,i-1} + ntu_{c,i}) \left(\theta_{w,i} - \frac{\theta_{c,i}+\theta_{c,i-1}}{2}\right) + 2\alpha_{ci} NTU_i v_{c,i} (R - \frac{\theta_{c,i}+\theta_{c,i-1}}{2} + 1) =$$

$$\frac{\mu_{c.i}+\mu_{c,i-1}}{\mu_{c.i}} (\theta_{c,i-1} - \theta_{c,i}) \tag{6}$$

The following dimensionless parameters have been used in the above energy equations:

$$\theta = \frac{T - T_{c,in}}{T_{h,in} - T_{c,in}} \ , \quad \mathrm{R} = \frac{T_a - T_{h,in}}{T_{h,in} - T_{c,in}} \ , \quad \alpha_i = \frac{U_{o,i} A_{o,i}}{U_i A_i} \ , \quad \lambda_i = \frac{k_{w,i} A_c}{C_{min} L} \tag{7}$$

$$v_{h,i} = \frac{C_{min}}{C_{h,i}} \ , \quad v_{c,i} = \frac{C_{min}}{C_{c,i}} \ , \quad \mu_{h,i} = \frac{C_{h,i}}{C_{h,in}} \ , \quad \mu_{c,i} = \frac{C_{c,i}}{C_{c,in}} \tag{8}$$

$$ntu_{h,i} = (\frac{hA}{C})_{h,i} \ , \quad ntu_{c,i} = (\frac{hA}{C})_{c,i} \ , \quad NTU_i = \frac{U_i A_i}{C_{min}} \ , \quad \Delta \mathrm{X}_i = \frac{\Delta x_i}{L} \tag{9}$$

The energy balance equations are made nondimensional in order to improve the computational efficiency and reveal the inherent relationship between these physical quantities. Additionally, for multi-stream PFHEs with more than two passages, analogous equations can be derived according to the corresponding passage arrangement. In these expressions, $\theta$ developed by Kroeger [3] represents the dimensionless temperature of hot fluid, cold fluid and metal wall followed by the suffix, *h*, *c* and *w*, respectively.

The ratio of external conductance $U_o A_o$ to internal conductance $U_i A_i$, heat in-leak parameter $\alpha$, was used to determine the amount of heat in-leak from the surrounding. Meanwhile, *R* is used to measure the gap between ambient and operating temperature. In some previous researches, $\alpha$, depending on the insulating ability of the system and practical operating condition, is always used as an empirical factor. Barron [16] reported the value equal to 0.01 in the design of air liquefaction systems. Hausen [17] suggested the value as 0.003 in general operation conditions and 0.0001 in most cryogenic applications when the *NTU* is between 10 and 100. For the cryogenic heat exchanger with high vacuum and multi-layer insulation, the radiation parasitic would dominate heat losses from the environment. Considering the parasitic is driven by the temperature difference between ambient and local node temperature, $\alpha_i$, the differential heat in-leak parameter, is used to represent different level of radiation parasitics in different node locations:

$$\alpha_i = \frac{\sigma \varepsilon_m A_{o,i} (T_a^4 - T_i^4)}{U_i A_i} \tag{10}$$

The longitudinal conduction parameter, $\lambda$, is defined as a ratio of longitudinal wall heat

conduction per unit temperature difference to the heat capacity rate of the fluid per unit length. Closed form expressions for calculating heat exchanger ineffectiveness, $1-\varepsilon$, have been derived by Kroeger [3] for a wide range of $NTU$, $C_c/C_h$ and $\lambda$. However, because of simplifications of these complex equations for imbalanced flow, the capacity rate ratio, $C_c/C_h$, is restricted in the range $0.8 \leq C_c/C_h \leq 1.25$ to be acceptable for most engineering computations. For some kinds of cryogenic systems such as Claude and Brayton, imbalanced flow often occurs in heat exchangers as part of the high pressure stream is routed through the expander. Aminuddin [10] has given typical heat capacity rate ratios for reference in various cryogenic processes.

Assuming adiabatic ends for the wall, the boundary conditions specifying inlet temperatures for hot and cold fluid are expressed:

$$\theta_{h,0} = 1 \ , \quad \theta_{w,0} = \theta_{w,1} \tag{11}$$

$$\theta_{c,n} = 0 \ , \quad \theta_{w,n} = \theta_{w,n+1} \tag{12}$$

Effectiveness $\varepsilon$, defined as a ratio of the actual heat transfer rate based on the hot fluid to the maximum possible heat transfer rate, has been widely used as a measure of thermal performance of heat exchangers:

$$\varepsilon = \frac{C_h(T_{h,in}-T_{h,out})}{C_{min}(T_{h,in}-T_{c,in})} = \frac{1-\theta_{h,out}}{v_h} \tag{13}$$

To consider directly the reduction in the effectiveness due to heat in-leak and longitudinal conduction, degradation factor, $\tau$, is adopted:

$$\tau = \frac{\Delta\varepsilon}{\varepsilon} = \frac{\varepsilon_{\alpha=0,\lambda=0}-\varepsilon_{\alpha\neq0,\lambda\neq0}}{\varepsilon_{\alpha\neq0,\lambda\neq0}} \tag{14}$$

The core pressure drop in the *i*th section mainly including two components, the frictional pressure drop and the pressure drop due to the momentum rate change, can be expressed as [2]:

$$\Delta P_i = \frac{G^2}{2g_c}\left[\frac{4f}{D_h}\Delta x_i\left(\frac{1}{\rho}\right)_m + 2\left(\frac{1}{\rho_{exit}} - \frac{1}{\rho_{entrance}}\right)\right] \tag{15}$$

## 3. Results and discussion

### 3.1. Comparison with available experimental results

The proposed model can also be utilized to analyze the other heat exchangers with different structures. For instance, considering heat in-leak only takes place on the cold fluid side and there exists only two streams, the accuracy of this model can be briefly examined by comparing with experimental results from coiled tube in tube heat exchangers [9]. Fig. 2 illustrates the comparison between the experimental results and numerical predictions, assuming adiabatic end conditions and equal per side number of transfer units, $ntu_h = ntu_c$. It can be observed that the temperature distribution along the length of hot fluid shows a good match with the actual condition, while temperature predictions near the entrance of cold fluid are slightly lower than the actual values. As suggested by the author, the general, empirically obtained heat in-leak parameter, $\alpha$, which may be a variable along the length rather than a constant, tends to cause the error. Therefore, the differential heat in-leak parameters, $\alpha_i$, across the outside surface should be considered carefully depending on the specific circumstances.

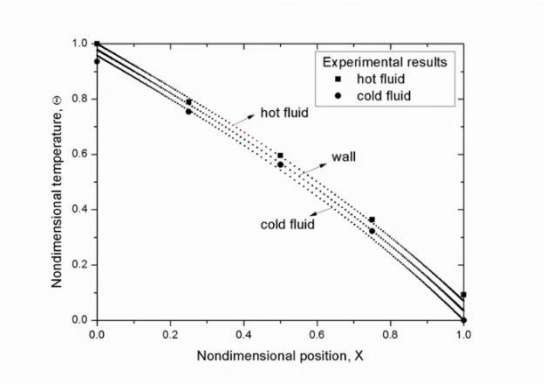


**Fig. 2.** Predictions of temperature distributions along the length of the heat exchanger

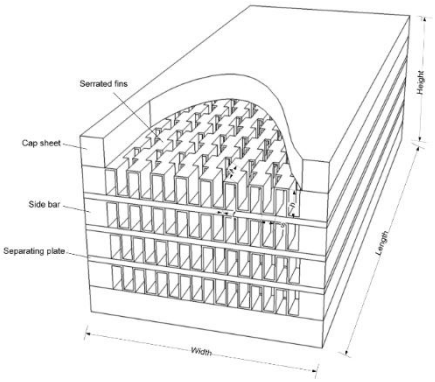


**Fig. 3.** Schematic view of a multi-channel PFHE core

### 3.2. Examination of numerical model

The generalized numerical model could be used to predict the performance of any multi-channel and multi-stream heat exchangers. The schematic view of the multi-channel PFHE is shown in Fig. 3 and the dimensions of the core and fins for model validation are given in Table 1. The side bar width, separating plate thickness and cap sheet thickness are set as 25, 1 and 6 mm, respectively. Two cases with the selected operation parameters from a helium refrigerator, as shown in Table 2, are used to analyze the flexibility and robustness of this model. Case-1 is set as a two stream heat exchanger to study the effects due to the dramatic physical changes of helium below 20K. Case-2 is a three stream heat exchanger with 6 layers for the hot stream and 2, 3 layers for the other cold streams respectively. The outer surfaces of heat exchangers are covered with multi-layer insulation to keep a low emissivity, 0.0045, and exposed to radiation from the thermal shield at 77 K.

**Table 1**
Details of the heat exchanger core and fins

| | Case 1 | | Case2 | | |
|---|---|---|---|---|---|
| Stream number | A | B | A | B | C |
| Fin type | Serrated | | Serrated | | |
| Fin height (mm) | 4.7 | 9.5 | 4.7 | 9.5 | 9.5 |
| Fin space (mm) | 2 | 1.4 | 2 | 1.4 | 1.4 |
| Fin thickness (mm) | 0.3 | 0.2 | 0.3 | 0.2 | 0.2 |
| Interrupted length (mm) | 3 | 3 | 3 | 3 | 3 |
| Core width (mm) | 250 | | 250 | | |
| Core length (mm) | 500 | | 1200 | | |
| Matrix metal | Aluminum 3003 | | | | |

**Table 2**
Operation conditions for case studies

| Case number | Stream number | Working fluid | Mass flow rate (g/s) | Inlet temperature (K) | Inlet pressure (kPa) | Number of layers | Layer pattern |
|---|---|---|---|---|---|---|---|

| | | | | | | | |
|---|---|---|---|---|---|---|---|
| 1 | A | Helium | 18 | 20 | 200 | 3 | A-B-A-B-A |
| | B | Helium | 18 | 4.7 | 120 | 2 | |
| 2 | A | Helium | 30 | 80 | 1920 | 5 | A-C-A-B-A-C-A -B-A-C-A |
| | B | Helium | 8 | 13 | 420 | 2 | |
| | C | Helium | 24 | 13 | 128 | 3 | |

Thermal-physical properties of helium are obtained using HEPAK [18]. The thermal conductivity of Aluminum (AL3003) at low temperature is acquired via the empirical correlation from NIST [19]. The general accepted correlations presented by Manglik and Bergles [20] are adopted to predict heat transfer and pressure drop performance. For offset strip fins, extended surfaces are used to increase the total rate of heat transfer. The above high-dimensional nonlinear equations are iteratively solved by MATLAB and the calculation procedure is illustrated in Fig. 4.

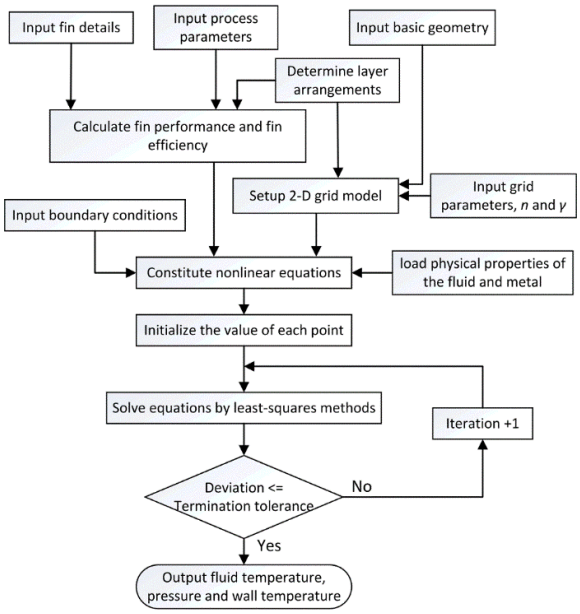


**Fig. 4.** Flow chart for the calculation procedure

To examine the accuracy of numerical prediction results, commercial software Aspen MUSE™ [12] are further applied to make comparisons. In the software, the heat leak is used to represent a heat empirical input from any source, therefore, it can't be acquired automatically and accurately. To take heat in-leak into consideration as well, 0.01% of the total heat transfer recommended by the engineering experience are input for two cases. The comparisons of the outlet temperature and pressure drop are illustrated in Table 3. It can be seen that the results calculated by Aspen MUSE™ agree well with the numerical predictions under similar conditions. Fig. 5 illustrates the lateral temperature profile at inlet, mid and outlet axial positions for eleven layers and ten separating walls as described in case-2. There exists a nonlinear temperature distribution at different axial positions to guarantee conduction heat transfer through the separating wall between the hot and cold fluids.

**Table 3**
Comparison results

| Case number | Stream number | Outlet temperature (K) | | Pressure drop (bar) | |
|---|---|---|---|---|---|
| | | Aspen MUSE | Numerical predictions | Aspen MUSE | Numerical predictions |
| 1 | A | 8.79 | 9.21 | 0.00175 | 0.00189 |
| | B | 15.45 | 15.01 | 0.00122 | 0.00130 |
| 2 | A | 18.05 | 18.94 | 0.00154 | 0.00160 |
| | B | 74.02 | 74.12 | 0.00149 | 0.00146 |

| | | | | | |
|---|---|---|---|---|---|
| | C | 73.19 | 71.66 | 0.01725 | 0.01688 |

### 3.3. Effect of property variations

For comparison, effectiveness curves in case-1 solved with actual local thermal-physical property variations and constant property parameters covering density, viscosity, specific heat and conductivity at the mean temperature are shown in Fig. 6. The increase of the core length, representing better heat transfer effect, causes a corresponding increase in the deviation between the results of two methods. It can be also seen from this figure, degradation curve declines due to weak influences of longitudinal conduction with the increase of the core length and limited effects of heat in-leak at the very low external emissivity.

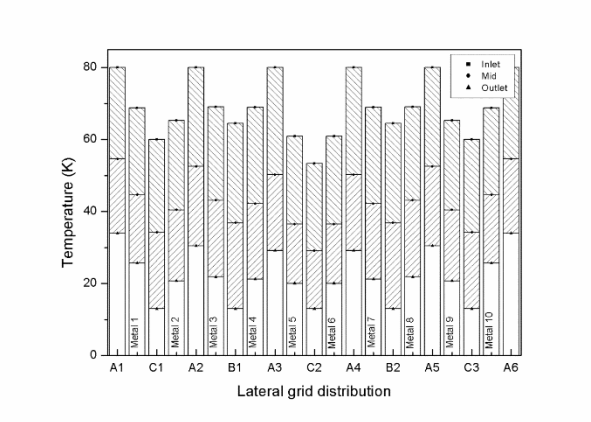


**Fig. 5.** Lateral temperature distribution at inlet, mid and outlet axial positions for Case-2

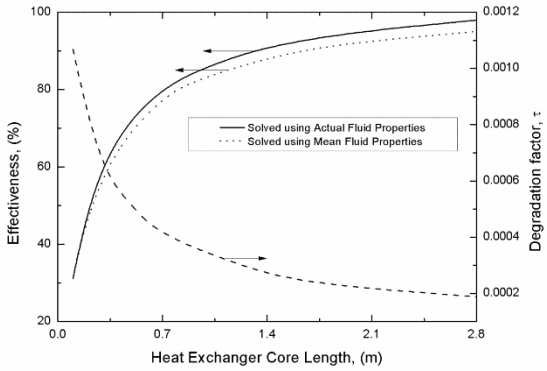


**Fig. 6.** Thermal performance of the heat exchanger versus core length calculated by variable and mean properties for Case-1

The influence curve of metal conductivity on the required heat exchanger core length under the condition of $\varepsilon = 0.8$ for case-1 is shown in Fig. 7. It can be seen that increasing metal conductivity couples with falling core length at the very low metal conductivity. Because the core length needs to be increased to make up the weak heat transfer ability to satisfy performance requirements. However, with metal conductivity gradually increasing, the core length remains almost unchanged due to the effect of longitudinal conduction begins to dominate and reduces heat transfer augmentation caused by the enhancement of metal thermal conductivity.

### 3.4. Effect of longitudinal conduction parameter, $\lambda$

Fig. 8 illustrates the effect of $\lambda$ on $\tau$ as a function of *NTU* under the condition of $ntu_h = ntu_c$, $\alpha = 0$ and $R = 0$ for balanced flow and imbalanced flow. For the case of adiabatic end conditions and no external heat transfer, the sensible heat exchange is identical for the hot and cold fluids. Although effectiveness increases with *NTU* due to available additional surface area, degradation curves based on $\lambda$ represent different trends for different flows. On the whole, the performance of the heat exchanger deteriorates with the increase of $\lambda$ as the conduction effect enhances. For balanced flow, $C_c/C_h$ =1, degradation curves approach asymptotic maximums at high *NTU*. In contrast, for unbalanced flow, $C_c/C_h$ =0.8 (1.25), degradation factors always reach the maximum at *NTU*=10

approximately, which is close to the common design value of cryogenic heat exchangers. It's worth noting, essentially similar trends are shown in degradation curves for $C_c/C_h$ =0.8 and $C_c/C_h$ =1.25 due to the equal ratio of minimum to maximum heat capacity rates.

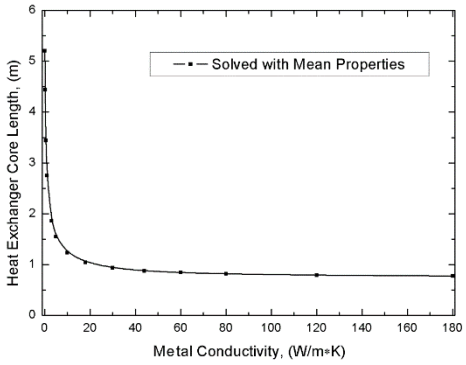


**Fig. 7.** The core length versus metal conductivity for Case-1 when $\varepsilon = 0.8$

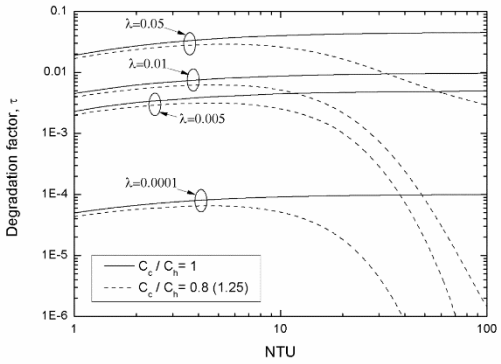


**Fig. 8.** Effect of longitudinal conduction parameter, $\lambda$, on degradation factor, $\tau$

### 3.5. Effect of heat capacity rate ratio, $C_c/C_h$ and heat in-leak parameter, $\alpha$

Two typical cases with the temperature ranging from 300 K to 80 K ($R = 0$) and a larger temperature difference between ambient and streams, from 80 K to 20 K ($R = 3.67$), are analyzed. Fig. 9 shows the distribution curves about the effect of $C_c/C_h$ on $\tau$ due to $\lambda$ and $\alpha$ in a comprehensive manner. Further deterioration can be obviously observed for major operating conditions at $C_c/C_h$ =1, as the temperature gradient across the length of the wall reaches the maximum. In particular, for $\alpha = 0.003$ and $\lambda = 0.001$, the degradation curve shows an ascending trend with the increase of $C_c/C_h$. This's because, $\alpha$, relative to $\lambda$, is sufficient enough to dominate the worsening effect of heat transfer for imbalanced flow. When $C_c/C_h$ increases, higher $C_c$ implies lower temperature for cold stream. With the assumption of only cold stream in the model exposed to external parasitic, heat in-leak enhances due to incremental temperature difference between ambient and cold stream.

Fig. 10 illustrates degradation curves with *NTU* for different $\alpha$ and $C_c/C_h$ for $\lambda = 0$, $R = 0$. With the increase of $\alpha$, the heat transfer performance is further deteriorated by the aggravation of poor insulation. It can be also observed that deterioration decreases at low *NTU*, as the corresponding external surface area under a fixed $\alpha$ value becomes small.

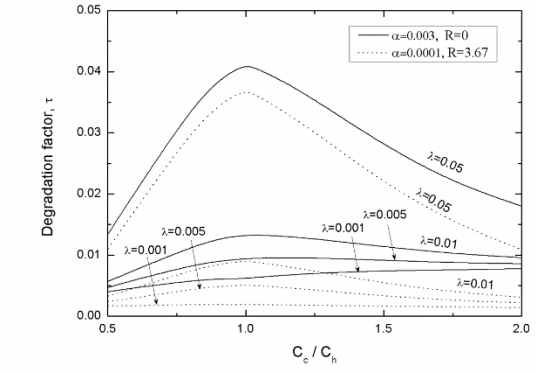


**Fig. 9.** Effect of capacity rate ratio, $C_c/C_h$

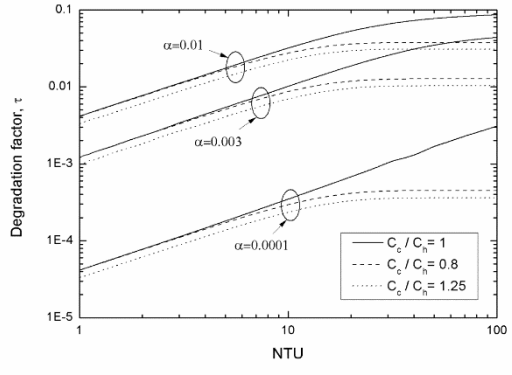


**Fig. 10.** Effect of heat in-leak parameter, $\alpha$, on , on

degradation factor, $\tau$ degradation factor, $\tau$ for R=0

In contrast, the heat exchanger is evaluated with a larger temperature difference between ambient and streams ($R = 3.67$) as illustrated in Fig. 11. It shows the same trend at very low *NTU* while the previous law about more severe deterioration occurred in balanced flow no longer applies. It's worth noting that the figure don't include higher *NTU*. Because cold fluid effectiveness is likely to exceed 100% above approximately *NTU*=6, as insufficient insulation may cause cold fluid to be heated warmer than the inlet hot fluid. Fig. 12 shows an example for $NTU = 20$, $\alpha = 0.01$, $C_c/C_h$ =1, $\lambda = 0$ and $R = 3.67$. Internal temperature cross can be observed due to the domination of external heat transfer.

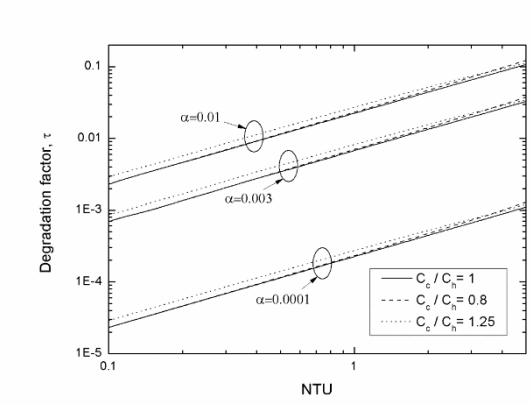


**Fig. 11.** Effect of heat in-leak parameter, $\alpha$, on degradation factor, $\tau$ for R=3.67

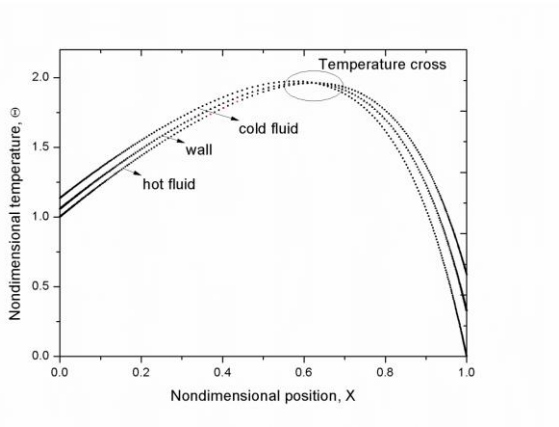


**Fig. 12.** Temperature distribution for $NTU = 20$, $\alpha = 0.01$, $C_c/C_h$ =1, $\lambda = 0$ and $R = 3.67$

## 4. Conclusions

The numerical model taking into account of various loss mechanisms including longitudinal heat conduction, heat in-leak from surroundings and property variations for counter-flow heat exchangers is developed in dimensionless form. This model can be successfully applied to calculate heat transfer and pressure drop performance of multi-stream PFHEs and evaluate deterioration caused by these losses comprehensively for cryogenic application. For comparisons with the results from Aspen MUSE$^{TM}$, two integrated cases in regard to multi-channel and multi-stream heat exchangers are calculated. The results obtained by this model are in good agreement with the software. Distinguishing from the software, the model can also calculate heat in-leak, rather than inputting an empirical value by experience, and predict the local temperature along the length for every fluid and metal wall. It can be found through this model: i. Significant deviations may occur in the results calculated by actual local thermal-physical property variations and constant property parameters. ii. For a specific case, there exists a conductivity value of available metal material at the low temperature, to satisfy performance requirements with the possible least heat exchanger length. iii. Performance deterioration enhances with significant $\alpha$ and $\lambda$ for cryogenic applications. In addition to operation at very low *NTU*, the degradation always reaches the maximum for balanced flow. iv. For some extreme cases with poor insulation, temperature cross would appear due to external heat transfer from surroundings dominating the system. v. The numerical model could be used in the design of cryogenic counter-flow heat exchangers and able to calculate under the actual operation conditions to evaluate heat transfer and

pressure drop performance.

**Nomenclature**

| | |
|---|---|
| $A$ | – heat transfer area, [$m^2$] |
| $A_0$ | – surface area exposed to ambient per unit length, [$m^2$] |
| $A_c$ | – cross-sectional area, [$m^2$] |
| $C$ | – heat capacity rate, $(= \dot{m}c_p)$, [$WK^{-1}$] |
| $c_p$ | – specific heat capacity, [$Jkg^{-1}K^{-1}$] |
| $D_h$ | – hydraulic diameter, [m] |
| $f$ | – Fanning friction factor, [–] |
| $G$ | – mass flux, [$kgm^{-2}s^{-1}$] |
| $g_c$ | – proportionality constant in Newton's second law of motion, [–] |
| $h$ | – heat transfer coefficient, [$Wm^{-2}K^{-1}$] |
| $i$ | – node index, [–] |
| $k$ | – thermal conductivity, [$Wm^{-1}K^{-1}$] |
| $L$ | – heat exchanger length, [m] |
| $\dot{m}$ | – mass flow rate, [$kgs^{-1}$] |
| $n$ | – number of elements along the length, [–] |
| $ntu$ | – number of transfer units per side, [–] |
| $NTU$ | – overall number of transfer units, [–] |
| $P$ | – pressure, [Pa] |
| $R$ | – dimensionless temperature gap defined in Eq. [7] |
| $T$ | – temperature, [K] |
| $U$ | – overall heat transfer coefficient, [$Wm^{-2}K^{-1}$] |
| $x$ | – axial coordinate, [m] |
| $X$ | – dimensionless axial coordinate, [–] |

*Greek symbols*

| | |
|---|---|
| α | – heat in-leak parameter defined in Eq. [7] |
| λ | – longitudinal conduction parameter defined in Eq. [7] |
| $\tau$ | – degradation factor defined in Eq. [14] |
| $\varepsilon$ | – effectiveness defined in Eq. [13] |
| $\rho$ | – density, [$kgm^{-3}$] |
| $\varepsilon_m$ | – effective emissivity, [–] |
| $\sigma$ | – Stefan–Boltzmann constant, [5.67e-8 $Wm^{-2}K^{-4}$] |
| $\gamma$ | – numerical parameter representing the grid concentration factor, [–] |
| $\mu, v$ | – capacity ratio defined in Eq. [8] |
| $\theta$ | – dimensionless temperature defined in Eq. [7] |
| $\eta_f$ | – fin efficiency, [–] |

*Subscripts*

| | |
|---|---|
| $a$ | – ambient |
| $c, h$ | – cold and hot fluid |
| $in, out$ | – inlet and outlet |
| $m$ | – mean value |
| $min$ | – minimum |
| $w$ | – separating wall |

**References**


[1] Kays, W. M., London, A. L., *Compact Heat Exchangers*, *3rd ed*, McGraw-Hill, New York, 1984

[2] Shah, R. K., Sekulic, D. P., *Fundamentals of Heat Exchanger Design*, Wiley, Hoboken (NJ), 2003

[3] Kroger, P. G., Performance deterioration in high effectiveness heat exchangers due to axial conduction effects, *Advances in Cryogenic Engineering, 12* (1967), pp. 363–72

[4] Narayanan, S. P., Venkatarathnam, G., Performance of a counterflow heat exchanger with heat loss through the wall at the cold end, *Cryogenics, 39* (1999), pp. 43–52

[5] Hansen, B. J., *et al*., Plate fin heat exchanger model with axial conduction and variable properites, *Advances in Cryogenic Engineering,* (2012) pp. 615-22

[6] Krishna, V., *et al*., Effect of longitudinal wall conduction on the performance of a three-fluid cryogenic heat exchanger with three thermal communications, *International Journal of Heat and Mass Transfer, 62* (2013) pp. 567-77

[7] Saberimoghaddam, A., Abadi, M. M. B. R., Influence of tube wall longitudinal heat conduction on temperature measurement of cryogenic gas with low mass flow rates, *Measurement, 83* (2016) pp. 20-8

[8] Chowdhury, K., Sarangi, S., Performance of cryogenic heat exchangers with heat leak from the surroundings, *Advances in Cryogenic Engineering, 29* (1984) pp. 273–80

[9] Gupta, P., Atrey, M. D., Performance evaluation of counter flow heat exchangers considering the effect of heat in leak and longitudinal conduction for low temperature applications, *Cryogenics,* 40 (2000) pp. 469–74

[10] Aminuddin, M., Zubair, S. M., Characterization of various losses in a cryogenic counterflow heat exchanger, *Cryogenics, 64* (2014) pp. 77-85

[11] Nellis, G. F., A heat exchanger model that includes axial conduction, parasitic heat loads, and property variations, *Cryogenics, 43* (2003) pp. 523–38

[12] AspenONE. Aspen MUSE, V7.2, Aspen Technology, www.aspentech.com

[13] Pacio, J. C., Dorao, C. A., A review on heat exchanger thermal hydraulic models for cryogenic applications, *Cryogenics, 51* (2011) pp. 366–79.

[14] Gupta, P. K., *et al*., Second law analysis of counter flow cryogenic heat exchangers in presence of ambient heat-in-leak and longitudinal conduction through wall, *International Journal of Heat and Mass Transfer, 50* (2007) pp. 4754–66

[15] Goyal, M., *et al*., Two dimensional model for multistream plate fin heat exchangers, *Cryogenics, 61* (2014) pp. 70-8

[16] Barron, R. F., Effect of Heat Transfer from Ambient on Cryogenic Heat Exchanger Performance, *Advances in Cryogenic Engineering, 29* (1984) pp. 265-72

[17] Hausen, H., *Heat transfer in counterflow, parallel flow and cross flow*, McGraw-Hill, New York, 1983

[18] Users guide to HEPAK, Version 3.4, Horizon Technologies, http://www.htess.com

[19] NIST Cryogenics Technologies Group, Material Properties, http://cryogenics.nist.gov/MPropsMAY/materia/properties.html

[20] Manglik, R. M., Bergles, A. E., Heat transfer and pressure drop correlations for the rectangular offset strip fin compact heat exchanger, *Experimental Thermal and Fluid Science, 10* (1995) pp. 171–80